PAPER

On the interaction of scrape off layer filaments

To cite this article: F Militello *et al* 2017 *Plasma Phys. Control. Fusion* **59** 125013

IOP Publishing Plasma Physics and Controlled Fusion
Plasma Phys. Control. Fusion 59 (2017) 125013 (11pp) https://doi.org/10.1088/1361-6587/aa9252

On the interaction of scrape off layer filaments

F Militello[1], B Dudson[2], L Easy[1,2], A Kirk[1] and P Naylor[2]

[1] CCFE, Culham Science Centre, Abingdon, Oxon, OX14 3DB, United Kingdom
[2] York Plasma Institute, Department of Physics, University of York, Heslington, York YO10 5DD, United Kingdom

E-mail: fulvio.militello@ukaea.uk

Received 20 July 2017, revised 21 September 2017
Accepted for publication 10 October 2017
Published 10 November 2017

Abstract

The interaction of L-mode and inter-ELM scrape-off layer (SOL) filaments is investigated by simulating the dynamics of two seeded density perturbations with different initial separation. A numerical campaign of 2D and 3D simulations is presented to explore the effect that different filaments' perpendicular size and relative distance have on their reciprocal action. It is shown that the interaction is weak unless the filaments are in close proximity, i.e. with a separation of the order of the filaments' diameter in the drift plane. The interaction occurs when the dipolar electrostatic fields associated with the filaments merge or cancel each other and it leads to changes in the radial velocity in the centre of mass of the system that are modest ($\leqslant 50\%$) and quickly decaying with separation. These results show that filaments travelling in the SOL can be considered to a good approximation as independent entities.

Keywords: SOL filaments, plasma exhaust, particle transport, SOL turbulence

(Some figures may appear in colour only in the online journal)

1. Introduction

Plasma transport in the boundary region of magnetically confined plasmas needs to be understood if reliable predictions for reactor relevant machines are to be achieved. Unfortunately, no first principle theory is yet available that can encompass all the relevant features of the turbulent environment that characterises the plasma exhaust. Extrapolations are therefore based on empirical scaling laws with limited theoretical understanding.

Experimental evidence [1–5] shows that the scrape off layer (SOL), the narrow region of plasma just outside the magnetic separatrix where the exhaust occurs, is dominated by coherent structures called filaments. The filaments play an important role in transporting the plasma particles at large distances from the separatrix, and therefore contribute to shape the time averaged density profile in the SOL. It is still unclear whether the confinement within L-mode and inter-ELM filaments is sufficiently efficient to allow these structures to propagate a significant amount of energy across the magnetic field. This is especially true in the inter-ELM phase of H-mode, although in L-mode infra-red measurements showed that they form spiral patterns of enhanced heat flux at the divertor target that extend into the far SOL [6].

Filaments have been observed in multiple machines and in all operating regimes. Three diagnostic approaches provided the majority of the experimental results available in literature: reciprocating or wall mounted Langmuir probes [1, 2, 7–12], fast visual cameras [3–5] and gas puff imaging [13–18]. In L-mode and in the inter-ELM phase, the filaments appear as density and temperature perturbations that are well aligned with the equilibrium magnetic field. Measurements in the so called far-SOL show that they are well spaced between each other (they are intermittent) and that they move through a rarefied and cold plasma [19].

The basic mechanism driving the cross field motion of the filaments is well understood in its general principles. It involves the formation of an electric field in response to the non-solenoidal diamagnetic current driven by the pressure gradients in the filament [20] and the consequent formation of an $\mathbf{E} \times \mathbf{B}$ drift that self-propels the perturbation in the radial direction. The detailed physics of the diamagnetic current closure (through parallel, polarisation or viscous currents) is more complicated but determines how the filament velocity

scales with respect to its features (e.g. amplitude above the background or perpendicular size). While approximate approaches shed some light on these details [20–22] a rigorous analytic nonlinear solution is still missing.

Simulations of SOL turbulence and of isolated filaments are used to fill this gap. Fully 3D simulations have emerged now as a new standard [23–29], while 2D simulations are still valuable for systematic scans at low computational cost [12, 30–33]. In both cases, the simulations showed a reasonable agreement with experimental measurements of SOL profiles and turbulence statistics [12, 21, 34, 35] as well as isolated filament motion [29, 36]. Despite the efforts of a growing community, several fundamental elements are still missing and a proper 3D simulation in full geometry of reactor relevant machines requires a very significant amount of computational resources.

As a consequence of the complexity of the nonlinear 3D simulations, reduced analytical models capturing the essential features of SOL transport might have an important role in predicting future behaviour in new machines. In recent years, a statistical model has been developed to correlate filament physics with single point properties of the turbulence [37]. This led to conclusions largely consistent with the experimental observations. Even more recently, this model was extended to generate a theoretical framework that allows correlating the statistics of the filaments with the approximate first principle knowledge of their motion with the features observed in the time averaged SOL profiles [38, 39]. This new theoretical framework was motivated by the observation that, in experimental analyses, a lot of attention is devoted to the mean SOL profiles, which are derived from a coarse time average of highly turbulent signals measured that show signatures of large intermittent events (the filaments).

One of the underlying assumptions of the statistical models discussed above is that filaments are not interacting and are moving independently from one other. From a technical point of view, this considerably simplifies the treatment, and makes analytic or semi-analytic treatments possible. In experimental measurements performed with visual cameras, the filaments seem to be well spatially separated both radially and toroidally, thus suggesting weak interactions. Also, measurements of the waiting time statistics at single points (typically at the walls) again suggest independence between filaments [40, 41]. However, all these measurements are unable to properly capture the interactions that large filaments might have with small (more difficult to detect) ones. Establishing a theoretical understanding of the level of interaction between filaments is therefore an important task in the perspective of developing simplified but reliable predictive modelling.

In this paper, we present a systematic study of the mutual interactions between a pair of isolated filaments. To this end, we performed 2D and 3D nonlinear simulations of seeded filaments with the STORM code [27, 28, 42] (which has been implemented using the BOUT++ framework [43]). A theoretical description of the expected interaction was also derived by approximating the electric field associated with the perturbations with electric dipoles. The relevance of our work is specific to L-mode and inter-ELM filaments, where net parallel plasma currents are negligible [3].

2. Initial estimates

We begin by introducing some general concepts and by developing a simplified approach to the problem we want to tackle. As mentioned in the Introduction, plasma filaments generate their own electric field, which is caused by the response to non-solenoidal (i.e. non-divergence free) diamagnetic currents flowing in the drift plane (i.e the plane locally perpendicular to the magnetic field, where particle and fluid drifts occur). It is through this electric field that filaments can potentially interact at a distance. Filaments can also generate a magnetic field due to the currents flowing through them, however, such fields are dipolar and weak [3] and are therefore not treated here (see the Conclusions section for more details).

For a pressure perturbation that has a roughly elliptical cross section in the drift plane, the electric potential is dipolar, with two lobes that can be asymmetric. Such an asymmetry induces a rotation of the filament in the bi-normal direction (i.e. perpendicular to both the radial and parallel directions) and can be caused by parallel pressure gradients, finite ion temperature effects or electron temperature perturbations [42].

In general, however, we can represent a filament as a roughly symmetric electric dipole, where the field is generated by a pair of long 'charged rods' aligned along the magnetic field rather than by point charges: $\mathbf{p}_\lambda = \lambda \mathbf{d}$, where λ is the average charge per parallel unit length accumulated in the two lobes and $\mathbf{d}$ is a vector passing through the centres of the two lobes and with magnitude equal to the distance between the centres. From basic electrodynamics, the electric field, $\mathbf{E}$, generated by a 'linear' dipole at the position $[r, \theta, z]$ in a cylindrical coordinate system centred on the dipole has the following form:

$$\mathbf{E}(r) = \frac{1}{2\pi\epsilon_0}\frac{2(\mathbf{p}_\lambda \cdot \hat{\mathbf{r}})\hat{\mathbf{r}} - \mathbf{p}_\lambda}{r^2}, \tag{1}$$

where $\hat{\mathbf{r}}$ is the radial unit vector. The force per unit length of a generic electric field on a dipole can be represented as:

$$\mathbf{f} = (\mathbf{p}_\lambda \cdot \nabla)\mathbf{E}. \tag{2}$$

From these equations it is straightforward to deduce the mutual force between a dipole $\mathbf{p}_1$ and a dipole $\mathbf{p}_2$ separated by a distance Δ, see appendix. In a Cartesian system where the z direction (along the filament) is negligible, the forces exchanged between two dipoles pointing vertically and upward (i.e. in the growing y direction), one located at the origin and the second at a generic position (x, y) are represented in figure 1. Here, the arrows show the direction of the mutual force and the colour-plot its magnitude. Note that the force between the dipoles decays rapidly, as $(x^2 + y^2)^{-3/2} = \Delta^{-3}$. The forces are mostly repulsive (i.e. f_x and/or f_y are directed away from the origin) and therefore tend to become weaker, while they are attractive only if $\arctan(|y/x|) > \pi/3$.

We can perform an order of magnitude calculation to determine the role of the the dipolar forces in the dynamics of the filaments. In order to affect the motion of the filament, the dipolar forces have to be at least comparable with the inertial

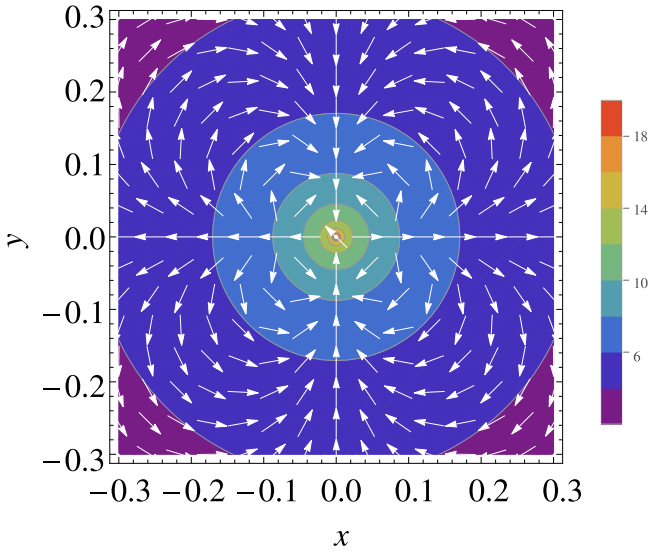

Figure 1. Force direction and normalised (logarithmic) intensity on a linear dipole positioned at (x, y) and generated by a second dipole located at the origin. Both dipoles are pointing in the positive y direction. The arrows have the same lengths as they only represent the direction of the force. The colour plot shows the magnitude of $\log[\pi\epsilon_0|\mathbf{f}|/(|\mathbf{p}_1||\mathbf{p}_2|)]$ and the x and y axes are in meters.

force acting on it. The latter can be estimated by noticing that the number density in a filament is around $n \approx 10^{19}\,\mathrm{m}^{-3}$, its radius is $w = 0.01$ m and hence the mass per unit length (in the parallel direction) of a typical filament is around:

$$m_i n \pi w^2 \approx 1.05 \times 10^{-11}\,\mathrm{kg\,m}^{-1} \tag{3}$$

(corresponding to a few hundreds of nanograms for a 10 m long filament, i.e. the weight of a grain of pollen or $\sim 1/2000$ of the plasma mass in the core), where $m_i = 3.34 \times 10^{-27}$ kg is the mass of deuterium. Here we took values relevant to MAST plasmas [44], which will be used also in the simulations. In the simulations presented in the next sections, we observe that the typical filament acceleration is around $(1\,\mathrm{km\,s}^{-1})/10^{-5}\,\mathrm{s} \approx 10^{8}\,\mathrm{m\,s}^{-2}$, hence the force on the filament per unit length is of the order of $10^{-3}\,\mathrm{N\,m}^{-1}$.

In order to estimate the dipolar force, we first estimate the electric field between the two charged rods representing the lobes. The filaments move radially because of an $\mathbf{E} \times \mathbf{B}$ drift [20], which generates a velocity of the order of 1%–5% of the sound speed [45], which in MAST corresponds to roughly $1\,\mathrm{km\,s}^{-1}$ [44, 46]. Taking a magnetic field of 1 T, we find that the filaments must generate an electric field, E, of the order of $1\,\mathrm{kV\,m}^{-1}$, which is also consistent with the estimate $\delta\phi \sim T_e/e$ and an electron temperature $T_e \sim 10$ eV. Such a field can be produced in the middle of two rods if their charge density is:

$$\lambda \approx 10^{-11} E w = 10^{-10}\,\mathrm{C\,m}^{-1} \tag{4}$$

which, estimating the distance between the lobes as the filament's diameter, leads to $|\mathbf{p}_\lambda| \approx 2 \times 10^{-12}$ C (remember this is a dipole per unit length).

We can now estimate the distance, Δ_{cr}, beyond which the dipolar electric force becomes weaker than the inertial force, i.e. Δ_{cr} such that $F_{\mathrm{dip}}(\Delta_{\mathrm{cr}}) = F_{\mathrm{in}}$ and $F_{\mathrm{dip}}(\Delta_{\mathrm{cr}}) \ll F_{\mathrm{in}}$ if $\Delta \gg \Delta_{\mathrm{cr}}$. By replacing the numbers above we obtain: $3.6 \times 10^{10}(2 \times 10^{-12})^2/\Delta^3 = 10^{-3}$. It follows that:

$$\Delta_{\mathrm{cr}} \approx (1.5 \times 10^{-10})^{1/3} \approx 5 \times 10^{-4}\,\mathrm{m}, \tag{5}$$

which is 20 times smaller that the width of the filament. We therefore deduce that the interactions between filaments should be very weak at distances longer than the characteristic perpendicular length scale of the filament. This is in agreement with the simulations discussed in the following section.

On the other hand, the dipole field approach is only correct in the limit $\Delta \gg w$. When filaments are separated by distances of the order of w their electric fields can be distorted, which results in an effect on the dynamics. In addition, the pressure perturbation associated with filaments in close proximity can be deformed thus changing their diamagnetic current and therefore their motion. In order to capture these effects, numerical simulations are required.

3. Description of the model

In order to have a quantitative understanding of the interaction between filaments, we simulated the nonlinear dynamics of two localised pressure perturbations in a simplified slab geometry, both in 3D (to have a full description of the physics) and in 2D (to perform a large number of high resolution scans). The amplitude, perpendicular size and relative position of the filaments was systematically varied in order to draw a complete picture of the phenomenon.

3.1. 3D equations

The 3D model we used is based on a drift reduction of two fluid equations with a Braginskii closure [47–49]. It was built in successive stages by gradually including new physical effects, see [22, 27, 28, 42, 44]. Note that the model now allows also for large density fluctuations as it does not make use of the Boussinesq approximation [50–52]. Our derivation of the generalised form of the vorticity follows [50] and assumes negligible effects from the curvature terms (i.e they are ordered small), an heuristic description of the viscous terms and small parallel ion velocities (which is the case apart from in the proximity of the target). The normalised equations are as follows:

$$\frac{\mathrm{d}\varpi}{\mathrm{d}t} = -U\nabla_\parallel \varpi - [v^2_{E\times B}/2, n] + \nabla_\parallel J_\parallel - \mathcal{C}(p) + \nabla\cdot\mu\nabla_\perp\varpi, \tag{6}$$

$$\frac{\mathrm{d}n}{\mathrm{d}t} = -\nabla_\parallel(nV) + n\mathcal{C}(\phi) - \mathcal{C}(p) + \nabla\cdot D\nabla_\perp n + S_n, \tag{7}$$

$$\frac{\mathrm{d}V}{\mathrm{d}t} = -V\nabla_\parallel V + \frac{m_i}{m_e}\left(\nabla_\parallel\phi - \frac{1}{n}\nabla_\parallel p + \eta_\parallel J_\parallel - 0.71\nabla_\parallel T\right) - \frac{S_n V}{n}, \tag{8}$$

$$\frac{\mathrm{d}U}{\mathrm{d}t} = -U\nabla_\parallel U - \nabla_\parallel\phi - \eta_\parallel J_\parallel + 0.71\nabla_\parallel T - \frac{S_n U}{n}, \tag{9}$$

$$\frac{3}{2}n\frac{\mathrm{d}T}{\mathrm{d}t} = -\frac{3}{2}nV\nabla_\parallel T - p\nabla_\parallel V + p\mathcal{C}\left(\phi - \frac{7}{2}T\right) - T^2\mathcal{C}(n) - \frac{m_e}{m_i}\frac{V^2}{2}\mathcal{C}(p) - \nabla_\parallel q_\parallel + \nabla\cdot\kappa_\perp\nabla_\perp T + 0.71J_\parallel\nabla_\parallel T - \eta_\parallel J_\parallel^2 + S_E + S_n\frac{m_e}{m_i}\frac{V^2}{2} - \frac{3}{2}S_nT. \quad (10)$$

Here $\varpi = \nabla\cdot(n\nabla_\perp\phi)$ is the generalised vorticity, ϕ is the electrostatic potential, n is the density ($n_e = n_i$), V and U are the electron and ion parallel velocities and T is the electron temperature. In addition, $\mathrm{d}f/\mathrm{d}t \equiv \partial f/\partial t + [f, \phi]$, $[f, g] = (\hat{\boldsymbol{b}}\times\nabla g)\cdot\nabla f$, $p = nT$, $J_\parallel = n(U - V)$, $\eta_\parallel = (m_e/m_i)\nu_\parallel/n$, $v_{E\times B} = |\hat{\boldsymbol{b}}\times\nabla\phi|$, $\nu_\parallel = 0.51\nu_{ei}/\Omega_i$ and $q_\parallel = -\kappa_{\parallel,0}T^{5/2}\nabla_\parallel T - 0.71TJ_\parallel$ with parallel thermal conductivity $\kappa_{\parallel,0} = 3.16(V_{\mathrm{th},e}^2/\nu_{ei})/D_B$ where ν_{ei} is calculated with n_0 and D_B is the Bohm diffusion coefficient. Assuming deuterium, $m_e/m_i = 1/3672$. The operator $\mathcal{C}$ represents curvature and leads to the interchange drive and its form will be discussed in section 3.3. S_n and S_E represent sources of particles and energy, respectively and produce a plasma background on top of which the filaments move [27]. Their mathematical representation and the equilibrium they generate is described in section 3.4. Finally, the collisional dissipative terms D, μ and $\kappa_\perp$ represent particle diffusivity, viscosity and heat conductivity. Their value was estimated using neoclassical theory as explained in [27, 34, 42].

The standard Bohm normalisation used for the equations and their boundary conditions are described in [27, 28, 42, 44] and are not discussed here for sake of brevity. In the following, all the quantities are to be considered normalised, unless otherwise stated.

3.2. 2D equations

In order to perform systematic scans with a higher resolution in the drift plane, we also developed a 2D isothermal version of equation (6)–(10) which is obtained by replacing the parallel physics terms with simplified scalar expressions. The 2D model is formed by the following equations:

$$\frac{\mathrm{d}\varpi}{\mathrm{d}t} = \frac{n(1 - \mathrm{e}^{-\phi})}{L} - [v_{E\times B}^2/2, n] - \mathcal{C}(n) + \mu\nabla_\perp^2\varpi, \quad (11)$$

$$\frac{\mathrm{d}n}{\mathrm{d}t} = \frac{n(1 - \mathrm{e}^{-\phi})}{L} - \frac{n - 1}{L} + n\mathcal{C}(\phi) - \mathcal{C}(n) + D\nabla_\perp^2 n. \quad (12)$$

Note that the source term in the density equation is replaced by $1/L$ on the right-hand side of equation (12), so that $n = 1$ at equilibrium. In addition, the normalised temperature is given by $T = 1$ due to the isothermal assumption. The model (11), (12) is an extension of the sheath dissipation closure discussed in [27] from which it removes the Boussinesq approximation [22].

3.3. Geometry and curvature

The simulations were performed in a straight slab geometry without magnetic shear. The extent of the numerical domain was several blob sizes ($\geqslant$10) in both the radial, x, and binormal, y, direction to reduce the effect of the boundary conditions. The perpendicular size of the domain, $[L_x, L_y]$, was [150, 100] for the 2D simulations, with a grid of 388×256 points, while for the 3D simulations we had [100, 100] and a coarser resolution of 128×128 points. In the 3D simulations, the parallel direction, z, covered the region between the midplane to the target, assuming symmetry around $z = 0$. We took $L_z = 5500$ and the grid contained 32 points. We reiterate that all the length are normalised, hence the quantities above are in units of ion sound Larmor radii, $\rho_s = \frac{\sqrt{T_0 m_i}}{eB_0}$, where e is the electron charge and B_0 the equilibrium magnetic field. For convenience, we take the binormal domain from $-L_y/2$ to $L_y/2$ so that the $y = 0$ plane divides it in half. However, it is more natural to take the x and z domains to go from 0 to $L_{x,z}$ as these are the directions in which the filament propagates.

Terms representing the curvature were artificially introduced and assumed a large aspect ratio approximation. Hence we define $\mathcal{C}(f) \equiv g\partial f/\partial y$, where $g = 2\rho_s/R$ and R is the major radius of the machine we intend to represent.

Note that in the 3D simulations, we impose symmetry boundary conditions at $z = 0$ and sheath boundary conditions at $z = L_z$, see [27, 28, 42, 44] for details.

3.4. Background equilibrium and source terms

The background plasma in which filaments move can affect their motion [20–22, 27]. In our 3D simulations, we generated a 1D background equilibrium by using appropriate particle and energy sources. We assumed homogeneity in the drift planes and took characteristic density and temperature corresponding to the midplane reference values, n_0 and T_0. The background was determined by the following sources:

$$S_n(z) = C_1\frac{10e^{\frac{10z}{L_\parallel}}}{L_\parallel(e^{10} - 1)}, \quad (13)$$

$$S_E(z) = C_2\frac{e^{-\frac{5z}{L_\parallel}}}{L_\parallel}, \quad (14)$$

where C_1 and C_2 were adjusted until the midplane value (at $z = 0$) of the normalised density and temperature reached 1 (which gave $C_1 = 0.71$ and $C_2 = 14.06$). These sources were employed previously in similar studies of isolated filament dynamics [27, 28, 44].

3.5. Filament initialisation

The seeded filaments were initialised by adding a density perturbations on top of the equilibrium field discussed in the previous subsection. The form of these perturbation was taken as follows:

$$\delta n = A_n\mathrm{e}^{-\frac{(x-x_0)^2+(y-y_0)^2}{w^2}}P(z) \quad (15)$$

which represents a Gaussian envelope in the drift plane with a circular shape centred at (x_0, y_0) and characterised by a scale length w (the width of the filament). In 3D simulations, we used $P(z) = \frac{1}{2}\left[1 - \tanh\left(\frac{z-L}{\delta_z}\right)\right]$ with $L = L_z$ and $\delta_z = 0.1L_z$. The 2D simulations, cannot have any z dependence, hence $P(z) = 1$. The amplitude of the filaments above the background was $A_n = 4$. All other fields were not perturbed at the beginning of the simulations (but a temperature perturbation did arise in 3D).

In most of the simulations, two filaments were 'vertically' or 'horizontally' aligned with a distance between their centres corresponding to $\epsilon = [1.5, 2, 3, 5]$ times the sum of their widths. In the 'vertical' alignment, this meant that $y_{0,A} = \epsilon_i(w_A + w_B)/2$ and $y_{0,B} = -\epsilon_i(w_A + w_B)/2$ while $x_{0,A} = x_{0,B} = 0.25L_x$ where the A and B subscripts label the two filaments. In the 'horizontal' configuration, $y_{0,A} = y_{0,B} = 0$, $x_{0,A} = 0.25L_x$ and $x_{0,B} = x_{0,A} + \epsilon_i(w_A + w_B)$, i.e. filament B is in front of filament A in this configuration.

We combined filaments of different width to investigate how relative sizes can affect the interaction. In particular, we used normalised widths w equal to 2.5, 5 and 7.5, which correspond to realistic sizes observed in MAST [46]. It is useful to notice that the normalised critical size separating the inertial from the sheath regime of filament dynamics is $w_* \approx 7.6$ for the parameters used in our simulations [22, 27, 53, 54]. This implies that, using a Pade' approximation, the maximum radial velocity is attained at $w_m \approx 7.6/2^{4/5} \approx 4.4$, as explained in [39].

Not all the combinations described above will be discussed, as some of them would be affected by the boundaries of the numerical domain. In particular, $w_A = w_B = 7.5$ with a vertical separation $\epsilon = 5$ leads to an artificial interaction through the periodic y boundary. Also, the horizontal domain is relatively short in 3D (but not in 2D), so that the out-most filament reaches the radial boundary early in the simulation (i.e. $t \leqslant 350$) if $w_B = 7.5$ with vertical separation $\epsilon = 5$. The same happens if $w_A = w_B = 7.5$ and $\epsilon = 3$ and if $w_A = 7.5$ and $w_B = 5$ and $\epsilon = 3$. These seven cases (out of the 72 possible) will not be included in our discussion. We have kept the results associated with cases where the interaction with the outer radial boundary occurs late in the simulation ($t \geqslant 500$) as most of the dynamics is well captured.

Finally, reference simulations were also performed with only one filament present. Their purpose was to provide unperturbed trajectories that could be compared with those of interacting filaments.

4. Numerical results

The simulations we performed investigated the interaction of two filaments initialised at different relative distances and sizes. 2D and 3D simulations were carried out, the former to perform a large number of high resolution scans, while the latter to assess the importance of non-isothermal effects and parallel dynamics.

The parameters used in all our simulations are representative of L-mode conditions at the edge of MAST plasmas [12, 44] and are as follows: $B_0 = 0.5T$ (toroidal), $T_0 = 20$ eV, $n_0 = 0.5 \times 10^{13}\,\mathrm{cm}^{-3}$, $R = 1.5$ m and the edge safety factor is $q = 7$.

4.1. 2D simulations

The general result of our simulation is that filaments interact only when they are in close proximity, i.e. the separation between their centres of mass needs to be shorter than a few diameters in order to see visible effects. If this is the case, the density perturbations can be significantly deformed and their motion, at least transiently, can be affected. As an example, we plot in figure 2 the time evolution of two representative cases in which interaction occurs, one with horizontal (i.e. radial) and one with vertical (i.e. bi-normal) separation.

In the horizontal configuration, whenever the filament at the back catches up with the one in front, the former tends to become elongated in the horizontal direction and the latter in the vertical. This is a result of the fact that the convective cells associated with the filaments combine and lead to a deformation of the density perturbations. In particular, the convective cells of the front filament effectively squeeze the back filament and pull it ahead. This is well represented in upper panels of figure 2 where the initial perturbations have the same amplitude and perpendicular size. If no interaction occurred, the filaments should have maintained their distance while travelling, however the simulation shows that the back filament reaches the front filament and is eventually absorbed in it. This evolution is quite typical of other initial configurations, as long as the initial separation is not too large ($\epsilon < 3$ for our parameters) and the velocity difference is not too large in favour of the front perturbation. The deformation induced in the filaments by the $\mathbf{E} \times \mathbf{B}$ velocity field seems to have a quite important role in this process. Indeed, the squeezing of the leading and trailing filaments, horizontal and vertical respectively, tend to slow down the former and speed up the latter [22] with the result that at the end of the simulation the density perturbations have merged and only one filament is present.

In the vertical configuration, when interaction occurs, a bridge of plasma roughly shaped like a horseshoe connects the filaments, see lower panel of figure 2, and the filaments tends to become more elongated in the vertical direction. After the bridge is formed, it is left behind by the filaments, as it does not have enough pressure to travel radially as fast as the main structures. In addition, density perturbations that are initially close to each other display a larger vertical separation as time passes. This general behaviour changes if small size perturbations ($w = 2.5$) are involved, as they seem to be vertically displaced and 'roped in' by the bridge in the wake of larger size filaments (this, however, requires close proximity, $\epsilon < 2$). This behaviour seems to be due to the fact that perturbations of a smaller size can be caught in one of the convective cells of a larger filament and therefore advected behind it.

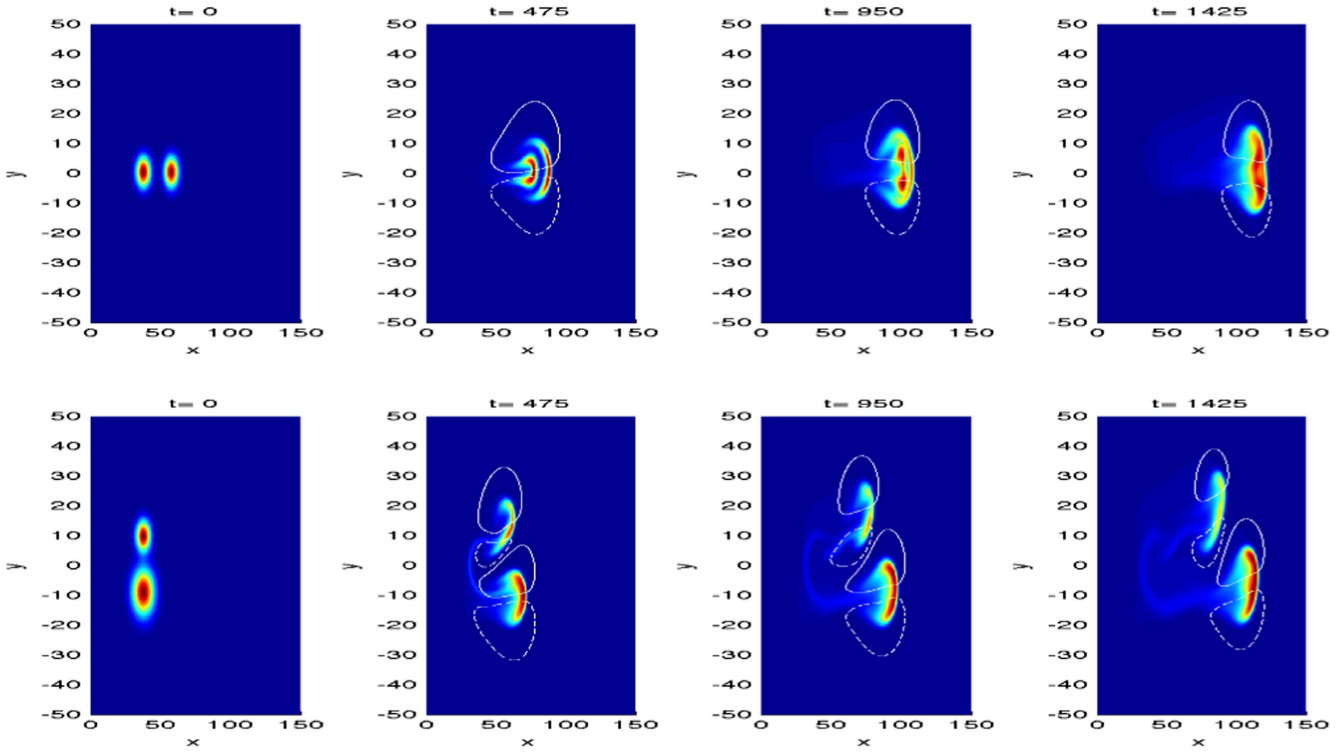

Figure 2. Time evolution of interacting filaments for two representative cases. In the upper panels, the initial separation is horizontal, $w_a = w_b = 5$ and $\epsilon = 2$. In the lower panels, the initial separation is vertical, $w_a = 5$, $w_b = 7.5$ and $\epsilon = 1.5$. The colour plots show how the density perturbation evolves at intervals separated by 475 normalised time units. Note that the colour bar is normalised to the maximum density in each frame in order to enhance the filaments' structures. White lines represent contours of ϕ at 0.1 and -0.1 (solid and dashed, respectively).

In order to quantify the effect of the interaction we need to identify useful figures of merit. The most obvious one is the radial velocity of the centre of mass of the system as it gives a measure of the cross field transport. First, for each simulation we have calculated the time dependent position of the centre of mass, defined as:

$$x_{\mathrm{cm}}(t) \equiv \frac{\int \mathrm{d}y \int x n(x, y, t) \mathrm{d}x}{\int \mathrm{d}y \int n(x, y, t) \mathrm{d}x}, \tag{16}$$

where the integrals are performed over the whole numerical domain (the vertical position y_{cm} can be calculated by replacing x with y in the numerator). The radial velocity of the centre of mass is simply obtained as $V_{x,\mathrm{cm}} = \mathrm{d}x_{\mathrm{cm}}/\mathrm{d}t$. To have a reference, we define a non-interacting centre of mass for the system. This can be done by performing two independent simulations initialised with only one filament in each (and therefore non-interacting by construction) and by calculating the centre of mass of the summed the density fields. In other words:

$$x_{\mathrm{cm,ref}}(t) \equiv \frac{\int \mathrm{d}y \int x [n_1(x, y, t) + n_2(x, y, t)] \mathrm{d}x}{\int \mathrm{d}y \int [n_1(x, y, t) + n_2(x, y, t)] \mathrm{d}x}, \tag{17}$$

where n_1 and n_2 are the density fields associated with the isolated filaments, initialised in such a way that $w = w_A$ for the first simulation and $w = w_B$ for the second.

Armed with this quantitative measure, an objective comparison between different simulations is possible. In figure 3, we show the time evolution of the radial velocity of the centre of mass for the 2D simulations with horizontal (solid curves) and vertical (dashed curves) filament separation respectively. For reference, circle markers show the non-interacting velocity calculated using $x_{\mathrm{cm,ref}}$.

In most cases, the interaction reaches its maximum, i.e. the greatest difference from the non-interacting reference, when the radial velocity is close to its peak. This period corresponds to more intense electrostatic fields associated with the filaments and stronger convection cells. However, this is not a general rule, as filaments merging after a relatively large initial separation also induce a strong perturbation in the dynamics. This can be observed, for example, in figure 3 for (w_A, w_B, ϵ) taking values (7.5, 2.5, 3) at $t = 500$–750 and (7.5, 5, 3) at $t = 500$–1000.

Note that curves representing large filaments with large horizontal separation can have a sharp drop towards the end of the simulation (compare e.g. $w_A = w_B = 7.5$, $\epsilon = 5$ at $t = 500$). This is due to the fact that the out-most filament reaches the outer boundary of the numerical domain and gets dissipated. This leads to the sudden reduction of the radial velocity of the centre of mass, but this is just a numerical artefact and should therefore be disregarded.

Comparing solid and dashed lines in figure 3, it is immediately clear that the interaction of horizontally separated filaments leads to a a speed up of their centre of mass, so that $V_{x,\mathrm{cm}} \geqslant V_{x,\mathrm{cm,ref}}$, where the non-interacting velocity of the centre of mass, $V_{x,\mathrm{cm,ref}}$, is defined by analogy with $V_{x,\mathrm{cm}}$.

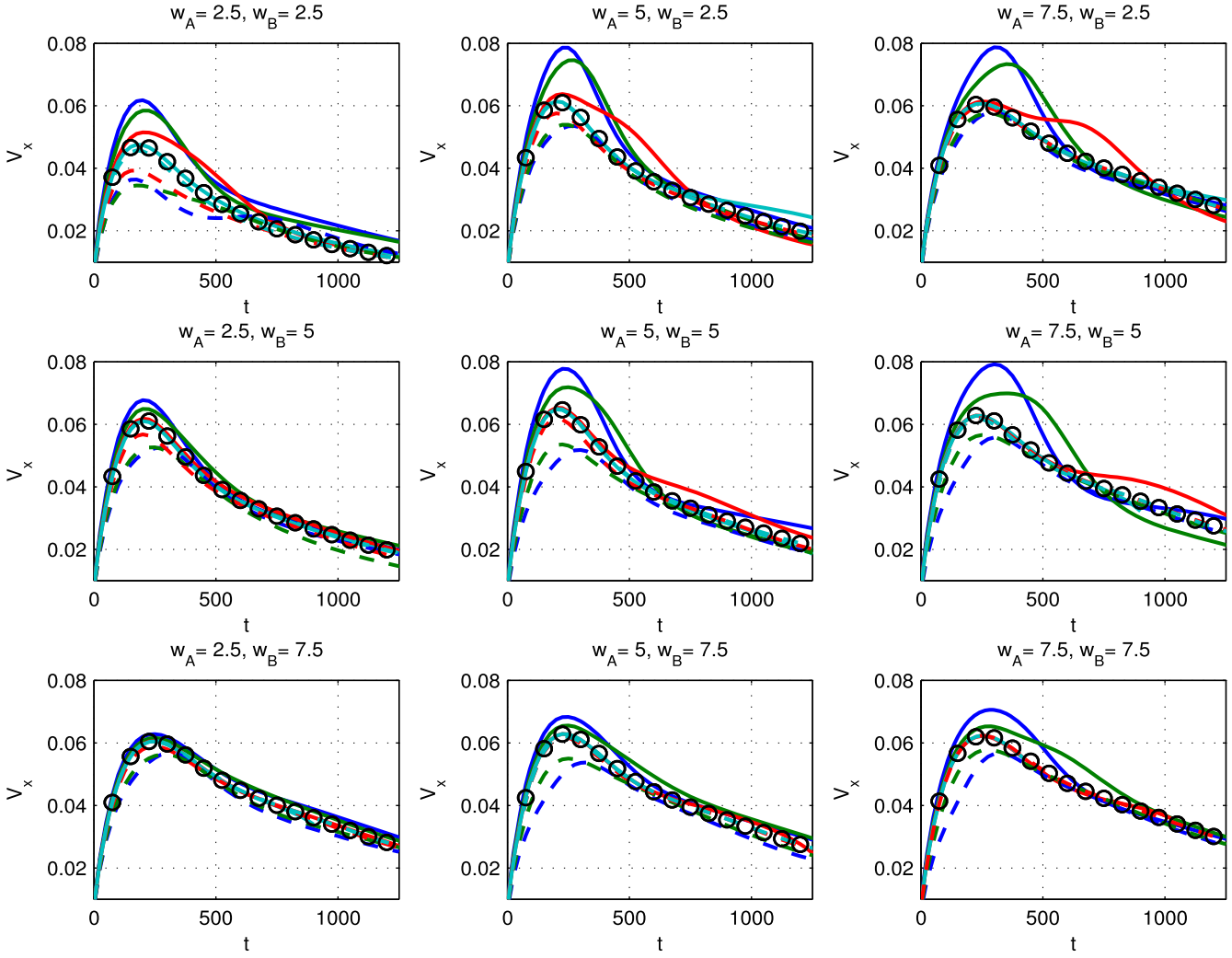

Figure 3. Time evolution of the radial velocity of the centre of mass of the two filaments. Blue, green, red and cyan curves represent ϵ equal to 1.5, 2, 3 and 5. Solid and dashed lines correspond to an initial horizontal and vertical separations, respectively. Black circles show the reference velocity of a single, not interacting filament.

Vertically separated filaments, on the other hand, show the opposite behaviour, with $V_{x,\mathrm{cm}} \leqslant V_{x,\mathrm{cm,ref}}$. This can be explained by the fact that merging filaments also merge their convective cells, thus increasing the $\mathbf{E} \times \mathbf{B}$ drive of the filament. Symmetrically, when the displacement is vertical, the convective cells between the density perturbations rotate in opposite direction and hence the electrostatic potential tends to cancel out, thus reducing the speed of the system. This also explains why the filaments tend to vertically separate as this cancellation creates an asymmetric configuration in the dipole which induces a poloidal component in the motion of the filaments (see bottom panels of figure 2).

In general, however, $V_{x,\mathrm{cm}}$ is only marginally different from $V_{x,\mathrm{cm,ref}}$, even when the interaction is the strongest. Indeed, figure 4 shows that the variation of the maximum velocity, $\Delta V_{\%} \equiv 100[\max(V_{x,\mathrm{cm,ref}}) - \max(V_{x,\mathrm{cm}})] \,/ \max(V_{x,\mathrm{cm}})$, does not exceed 40%–50% of the unperturbed value even for close proximity, i.e. $\epsilon = 1.5$, and tends to vanish for $\epsilon \geqslant 5$ in all the cases investigated. In other words, filaments always interact very weakly and even when they do, their shape is affected but the radial transport associated with them does not change significantly.

Finally, note that the dynamics resulting from the interaction is different when swapping the position of filaments of different widths. While this is obvious for the horizontal case (the velocity of two chasing filaments depends on their width), also for the vertical configuration is affected by this. This is due to the fact that the dipolar structure in the filaments is not exactly symmetric, i.e. upper and lower lobes of the potential have different intensities. This can be due to a number of factors such as the nonlinearity of the sheath boundary conditions, the presence of parallel gradients or the presence of temperature perturbations (see e.g. [42]). In our case, both parallel gradients and temperature perturbations are weak, hence the asymmetry in the potential is not very marked and swapping the filaments has a limited effect.

4.2. 3D simulations

The 3D simulations were performed to verify that parallel dynamics and thermal effects did not significantly change the

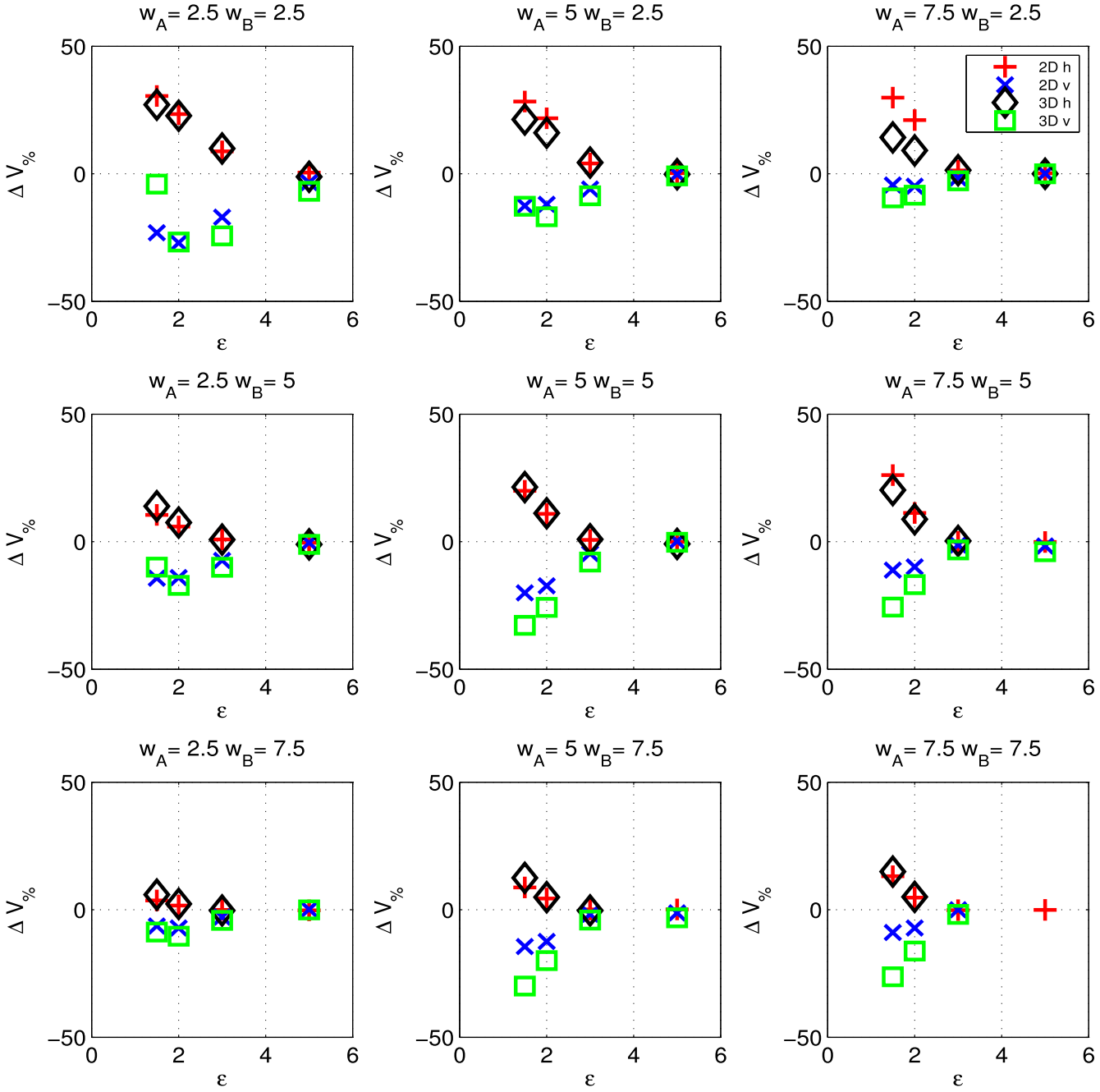

Figure 4. Variation of the maximum velocity, $\Delta V_{\%}$ with respect to reference case as a function of the separation of the filaments. Each frame represents a different combination of filament sizes. Crosses and plus (squares and diamonds) markers correspond to 2D (3D) simulations with initial vertical and horizontal separation respectively. Cases with strong interactions with the boundaries are not shown (see e.g. $w_A = w_B = 7.5$).

picture in the previous section. This was indeed the case, as the qualitative agreement with the 2D simulations was good. In particular, all the trends observed in the 2D simulations were successfully reproduced also in 3D, thus reinforcing the generality of our conclusions, see figure 4 for a comparison of the values of $\Delta V_{\%}$. A remarkable similarity is found when calculating $\Delta V_{\%}$ on drift planes at different parallel positions, thus implying that the discussion of the midplane results is sufficient to describe the 3D simulations.

Also the evolution of the shape of the filaments was not significantly altered by the 3D geometry. This is shown in figure 5, where we reproduce in 3D at $t = 875$ the same pairs of filaments represented in figure 2. Also here the background equilibrium is subtracted and the colour bar goes from zero to the maximum value of the density perturbation in the 3D field at that time. Both the coalescence of horizontally displaced filaments and the formation of a bridge structure in the vertically displaced cases were replicated.

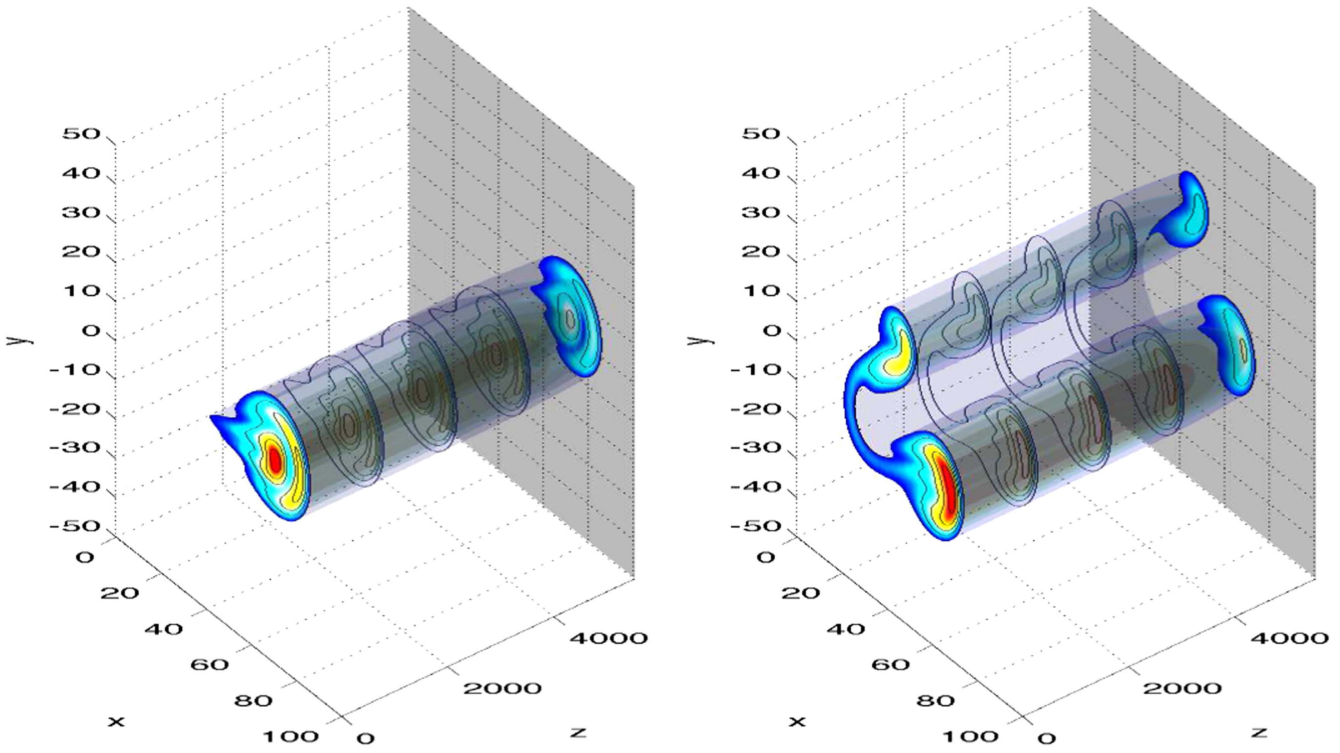

Figure 5. Same filaments as in figure 2 in 3D for $t = 875$ (colour bar normalised to the maximum density). The shaded region in the back represents the target.

5. Discussion and conclusions

Using simple estimates and numerical simulations we determined and characterised how pairs of SOL filaments interact with each other. We found that the dipolar electrostatic fields responsible for the motion of the filaments is too weak to play a significant role, unless the separation between the pressure perturbations is comparable with their width, i.e. they are in close proximity. If filaments are separated by more than 5 widths, their motion occurs as if they were completely isolated. Even when the perturbations are below this threshold, their dynamics, and most importantly the radial transport associated with them, remains almost unaffected, e.g. two filaments horizontally separated by one width have a radial velocity that is only $\sim$30% higher than the non-interacting reference case.

It is interesting at this point to discuss the average distance of filaments as measured in experimental conditions. Visual imaging of MAST plasmas shows that the SOL turbulence produces coherent structures that are almost regularly spaced toroidally. Detailed analysis shows that the perturbations have toroidal quasi-mode numbers that vary between 10 and 50 with a sharp peak at 30 [46]. On average, this means that the toroidal distance between filaments at the outer midplane is roughly $2\pi(90 + 60)/30 \approx 30$ cm. The inclination α of the field lines in MAST typically ranges between 30° and 45° [5, 46] at the outer midplane, hence the distance in the bi-normal direction is $30 \times \sin(\alpha)$, i.e. between 15 and 20 cm, which corresponds to roughly $7.5 \div 10$ typical filament's widths. These large pitch angles at the midplane are typical of spherical tokamaks due to their compact design. In general, however, smaller edge safety factors, i.e. stronger plasma currents, would produce a larger α and thus more separation. Conventional machines typically have $\alpha \sim 10$ degrees and hence filaments should be closer to each other if the toroidal separation is similar to the one observed in MAST. Measurements in Alcator C-Mod [16] suggest that the bi-normal separation is $\sim$4 filament's widths, thus smaller than in MAST, but still sufficient to ensure a weak interaction.

Assessing the radial separation between a filament and another is less straightforward. Reciprocating probe measurements suggest that the typical waiting time between signal bursts in the far SOL is around 100 μs [12] while visual imaging shows that filaments move at 1 km s^{-1}, hence their radial distance can be estimated at around 10 cm. This simple analysis of course has its limitations, since it does not account for the behaviour of perturbations not detected by visual cameras (because too small or too weak) and is less precise for the near SOL but it is nevertheless suggestive of the fact that filaments move rather independently from each other.

An alternative way to determine the filament separation is to use the intermittency parameter, $\gamma = \tau_d/\tau_w$, introduced in [37] and extended in [38, 39], which takes into account the ration between dwelling and waiting times of the filaments τ_d and τ_w respectively). The dwelling time, including the effect of the filament motion [38, 39], is given by $\tau_d^{-1} \approx \tau^{-1} + V/w$, where V is the filament velocity in the perpendicular plane and τ the characteristic draining time towards the divertor. We thus have that $1/\gamma \approx \tau_w/\tau + \epsilon$, where we have approximated $V\tau_w$ as the typical filament separation. Using MAST data from [12], in the far SOL $\tau_d \approx 15$ μs, $\tau_w \approx 100$ μs and $\tau \approx 1$ ms, from which we

estimate $\epsilon \approx 6$. Since the intermittency parameter increases towards the separatrix, we expect this to be an upper limit for ϵ.

These results support the idea that coherent structures in the SOL are generated by a Poisson process which describes independent events emitted stochastically at a constant rate. This assumption is at the base of recent theoretical models that predict the statistics of the SOL fluctuations and their correlation with the radial SOL profiles [37–39] and is also corroborated by experimental measurements of waiting times in long time series, which are exponentially distributed [40, 55]. In other words, the results presented in this paper provide the theoretical explanation for the observed lack of interaction between the filaments and at the same time justify on a first principle basis the use of simplified theoretical models for the estimation of the turbulence statistics in the SOL.

To conclude, it is useful to point out at the limitations of our approach. Our simulations are electrostatic, but we expect electromagnetic interactions if a net current were flowing in the filaments. This might be the case in ELM filaments, but typically L-mode and inter-ELM turbulent structures do not carry a significant parallel current [3, 56]. Theoretical models [20, 22] ascribe the motion of the filaments to a balance between parallel and perpendicular currents. These parallel currents, however, are predicted to have a dipolar structure, similar to the electrostatic field described in this paper. We therefore expect a shielding of the magnetic forces, and hence an effect on scales of a few widths only. For a thorough discussion of how ELM filaments (and holes) can interact through the net current they carry, see [57]. In our calculations, we assumed a fluid approximation, which is not justified for structures with a perpendicular size comparable with the Larmor radius. One could argue, however, that filaments would lose their coherence on such a small scale, as the plasma would not be properly confined. This might occur in the proximity of the separatrix at the X-point, where upstream filaments are stretched and peeled off by the effect of the magnetic shear [58–60]. Here, as they enter in divertor region, the tails of the filaments might have a significant interaction as the filaments pack close to one another. In the present work, we have not addressed the problem of how the filaments interact with a turbulent background (i.e. small amplitude perturbations in close proximity). However, based on our results, we expect that the weak electric fields associated with turbulent eddies should not significantly disturb the dynamics of large filaments. On the other hand, we know that a smooth background (i.e. fluctuation free time averaged profiles) can induce a (sheared) toroidal rotation of the filaments and determines their absolute velocity [27, 28]. Finally, correlations between turbulent structures can also occur due to their generation mechanism. In other words, filaments moving in the SOL might well maintain an imprint of the fully developed turbulence that generates them inside the separatrix. All these effects were not considered in our study and are left for future work.

Acknowledgments

FM acknowledges useful discussions with Dr N Walkden. We also thank Chris Ham for carefully reading the manuscript. This work has received funding from the RCUK Energy Programme [grant number EP/P012450/1]. The authors gratefully acknowledge support from the Archer computing resources under Plasma HEC consortium Grant No. EP/L000237/1. To obtain further information on the data and models underlying this paper please contact PublicationsManager@ukaea.uk.

Appendix. Analytic calculations

We derive here the analytic expression for the force generated by two linear dipoles (i.e. generated by couples of infinite parallel rods with constant charge per unit length). Using equations (1) and (2) we find that:

$$f_x = \frac{|\mathbf{p}_1||\mathbf{p}_2|}{\pi\epsilon_0\Delta^3}\{\sin(\gamma)\cos(\theta)[1 - 4\sin^2(\theta)] + \cos(\gamma)\sin(\theta)[1 - 4\cos^2(\theta)]\}, \quad \text{(A1)}$$

$$f_y = \frac{|\mathbf{p}_1||\mathbf{p}_2|}{\pi\epsilon_0\Delta^3}\{\sin(\gamma)\sin(\theta)[1 - 4\cos^2(\theta)] - \cos(\gamma)\cos(\theta)[1 - 4\sin^2(\theta)]\}. \quad \text{(A2)}$$

Without loss of generality, we chose a coordinate system such that the first dipole is located at the origin and is pointing in the positive y direction. θ is the (anti-clockwise) angle between the $x > 0$ axis and the line of length Δ connecting the origin and the second dipole, while γ is the angle between the two dipoles. Note that the modulus of the force does not depend on θ or on γ: $|f| \equiv \sqrt{f_x^2 + f_y^2} = \frac{|\mathbf{p}_1||\mathbf{p}_2|}{\pi\epsilon_0\Delta^3}$.

ORCID iDs

F Militello https://orcid.org/0000-0002-8034-4756
B Dudson https://orcid.org/0000-0002-0094-4867

References

[1] Antar G Y, Krasheninnikov S I, Devynck P, Doerner R P, Hollmann E M, Boedo J A, Luckhardt S C and Conn R W 2001 *Phys. Rev. Lett.* **87** 065001
[2] Antar G Y, Counsell G, Yu Y, Labombard B and Devynck P 2003 *Phys. Plasmas* **10** 419
[3] Kirk A *et al* 2006 *Plasma Phys. Control. Fusion* **48** B433
[4] Dudson B D, Ben Ayed N, Kirk A, Wilson H R, Counsell G, Xu X, Umansky M, Snyder P B and LLoyd B 2008 *Plasma Phys. Control. Fusion* **50** 124012
[5] Ben Ayed N, Kirk A, Dudson B, Tallents S, Vann R G L and Wilson H R 2009 *Plasma Phys. Control. Fusion* **51** 035016
[6] Thornton A J, Fishpool G and Kirk A 2015 *Plasma Phys. Control. Fusion* **57** 115010
[7] Boedo J A *et al* 2001 *Phys. Plasmas* **8** 4826
[8] Rudakov D L *et al* 2002 *Plasma Phys. Control. Fusion* **44** 717

[9] Boedo J A *et al* 2003 *Phys. Plasmas* **10** 1670
[10] Garcia O E, Horacek J, Pitts R A, Nielsen A H, Fundamenski W, Naulin V and Juul Rasmussen J 2007 *Nucl. Fusion* **47** 667
[11] Garcia O E, Pitts R A, Horacek J, Madsen J, Naulin V, Nielsen A H and Rasmussen J J 2007 *Plasma Phys. Control. Fusion* **49** B47
[12] Militello F, Tamain P, Fundamenski W, Kirk A, Naulin V and Nielsen A H 2013 *Plasma Phys. Control. Fusion* **55** 025005
[13] Zweben S J *et al* 2002 *Phys. Plasmas* **9** 1981
[14] Terry J L *et al* 2003 *Phys. Plasmas* **10** 1739
[15] Myra J R, D'Ippolito D A, Stotler D P, Zweben S J, LeBlanc B P, Menard J E, Maqueda R J and Boedo J 2006 *Phys. Plasmas* **13** 092509
[16] Grulke O, Terry J L, LaBombard B and Zweben S J 2006 *Phys. Plasmas* **13** 012306
[17] Zweben S J *et al* 2015 *Nucl. Fusion* **55** 093035
[18] Zweben S J, Myra J R, Davis W M, D'Ippolito D A, Gray T K, Kaye S M, LeBlanc B P, Maqueda R J, Russel D A and Stotler D P 2016 *Plasma Phys. Control. Fusion* **58** 044007
[19] LaBombard B, Boivin R L, Greenwald M, Hughes J, Lipschultz B, Mossessian D, Pitcher C S, Terry J L and Zweben S J 2001 *Phys. Plasmas* **8** 2107
[20] Krasheninnikov S I 2001 *Phys. Lett.* A **283** 368
[21] Garcia O E, Bian N H and Fundamenski W 2006 *Phys. Plasmas* **13** 082309
[22] Omotani J, Militello F and Easy L 2015 *Plasma Phys. Control. Fusion* **58** 014030
[23] Angus J R, Umansky M V and Krasheninnikov S I 2012 *Phys. Rev. Lett.* **108** 215002
[24] Walkden N R, Dudson B D and Fishpool G 2013 *Plasma Phys. Control. Fusion* **55** 105005
[25] Ricci P, Riva F, Theiler C, Fasoli A, Furno I, Halpern F D and Loizu J 2015 *Phys. Plasmas* **22** 055704
[26] Tamain P, Bufferand H, Ciraolo G, Colin C, Ghendrih P, Schwander F and Serre E 2014 *Contrib. Plasma. Phys.* **54** 555
[27] Easy L, Militello F, Omotani J, Dudson B, Havlíčková E, Tamain P, Naulin V and Nielsen A H 2014 *Phys. Plasmas* **21** 122515
[28] Easy L, Militello F, Omotani J and Dudson B 2016 *Phys. Plasmas* **23** 012512
[29] Militello F *et al* 2016 *Plasma Phys. Control. Fusion* **58** 105002
[30] Garcia O E, Naulin V, Nielsen A H and Rasmussen J J 2004 *Phys. Rev. Lett.* **92** 165003
[31] Russell D A, Myra J R and D'Ippolito D A 2009 *Phys. Plasmas* **16** 122304
[32] Militello F, Fundamenski W, Naulin V and Nielsen A H 2012 *Plasma Phys. Control. Fusion* **54** 095011
[33] Militello F, Naulin V and Nielsen A H 2013 *Plasma Phys. Control. Fusion* **55** 074010
[34] Fundamenski W, Garcia O E, Naulin V, Pitts R A, Nielsen A H, Rasmussen J J, Horacek J and Graves J P 2007 *Nucl. Fusion* **47** 417
[35] Myra J R *et al* 2011 *Phys. Plasmas* **18** 012305
[36] Riva F *et al* 2016 *Plasma Phys. Control. Fusion* **58** 044005
[37] Garcia O E 2012 *Phys. Rev. Lett.* **108** 265001
[38] Militello F and Omotani J T 2016 *Nucl. Fusion* **56** 104004
[39] Militello F and Omotani J T 2016 *Plasma Phys. Control. Fusion* **58** 125004
[40] Garcia O E, Fritzner S M, Kube R, Cziegler I, LaBombard B and Terry J L 2013 *Phys. Plasmas* **20** 055901
[41] Walkden N R, Wynn A, Militello F, Lipschultz B, Matthews G, Guillemaut C, Harrison J and Moulton D 2017 *Nucl. Fusion* **57** 036016
[42] Walkden N R, Easy L, Militello F and Omotani J T 2016 *Plasma Phys. Control. Fusion* **58** 115010
[43] Dudson B D, Umansky M, Xu X, Snyder P and Wilson H 2009 *Comput. Phys. Commun.* **180** 1467
[44] Militello F, Garzotti L, Harrison J, Omotani J T, Scannell R, Allan S, Kirk A, Lupelli I and Thornton A J 2016 *Nucl. Fusion* **56** 016006
[45] Terry J *et al* 2005 *J. Nucl. Mater.* **337–339** 322
[46] Kirk A, Thornton A J, Harrison J R, Militello F and Walkden N R 2016 *Plasma Phys. Control. Fusion* **58** 085008
[47] Braginskii S I 1965 *Rev. Plasma Phys.* **1** 205
[48] Zeiler A, Drake J F and Rogers B 1997 *Phys. Plasmas* **4** 2134
[49] Simakov A N and Catto P J 2003 *Phys. Plasmas* **10** 4744
[50] Angus J R and Krasheninnikov S I 2014 *Phys. Plasmas* **21** 112504
[51] Russell D A, D'Ippolito D A and Myra J R 2012 On relaxing the Boussinesq approximation in scrape-off layer turbulence (SOLT) model simulations *Bulletin of the American Physical Society, 54th Annual Meeting of the APS Division of Plasma Physics* vol 57
[52] Halpern F D, Ricci P, Jolliet S, Loizu J, Morales J, Mosetto A, Musil F, Riva F, Tran T M and Wersal C 2016 *J. Comput. Phys.* **315** 388
[53] Yu C X, Gilmore M, Peebles W A and Rhodes T L 2003 *Phys. Plasmas* **10** 2772
[54] Theiler C, Furno I, Ricci P, Fasoli A, Labit B, Müller S H and Plyushchev G 2009 *Phys. Rev. Lett.* **103** 065001
[55] Garcia O E, Horacek J and Pitts R 2015 *Nucl. Fusion* **55** 062002
[56] Vianello N *et al* 2011 *Phys. Rev. Lett.* **106** 125002
[57] Myra J R 2007 *Phys. Plasmas* **14** 102314
[58] Farina D, Pozzoli R and Ryutov D D 1993 *Nucl. Fusion* **33** 1315
[59] Cohen R H and Ryutov D D 2006 *Contrib. Plasma Phys.* **46** 678–84
[60] Harrison J R, Fishpool G M, Thornton A J, Walkden N R and MAST Team 2015 *Phys. Plasmas* **22** 092508